Measurement of the Growth Kinetics of Microdomains Binary n-Alkane Solid Solutions by Infrared Spectroscopy

ARTICLE *in* THE JOURNAL OF PHYSICAL CHEMISTRY · NOVEMBER 1992

Impact Factor: 2.78 · DOI: 10.1021/j100203a078

5 AUTHORS, INCLUDING:

Herbert L. Strauss
University of California, Berkeley
179 PUBLICATIONS **6,355** CITATIONS

Measurement of the Growth Kinetics of Microdomains in Binary *n*-Alkane Solid Solutions by Infrared Spectroscopy

R. G. Snyder,* M. C. Goh,† V. J. P. Srivatsavoy, H. L. Strauss,

Department of Chemistry, University of California, Berkeley, California 94720

and D. L. Dorset

Medical Foundation of Buffalo, Buffalo, New York 14203 *(Received: May 6, 1992; In Final Form: September 3, 1992)*

Microphase segregation occurs in certain solid-solution binary mixtures of *n*-alkanes at room temperature. The kinetics of segregation for the mixtures $C_{28}{}^H/C_{36}{}^D$, $C_{29}{}^H/C_{36}{}^D$, and $C_{30}{}^H/C_{36}{}^D$ have been studied at molar concentration ratios of 4:1, 1:4, and 1:1. During the demixing, the mixture maintains a lamellar, highly crystalline orthorhombic subcell structure that is very similar to that of the pure odd-numbered *n*-alkanes. The average domain sizes of the segregated components of mixtures, in which one component is hydrogenated and the other deuterated, were determined from the band splitting observed for the infrared-active methylene-scissors band. The range of domain sizes that can be monitored extends from single isolated chains to aggregates of the order of 100–150 chains. Curves obtained from plotting log L against log t, where L is the average lateral dimension of the domains and t is time, are nonlinear. However, for mixtures of a given concentration ratio the curves vary in shape with chain length in a systematic way so as to correspond to different segments of a common (S-shape) curve. The relative rates of segregation for the different mixtures are, as expected, very sensitive to the chain-length difference between the two components. The rate increases dramatically as the chain-length difference increases. In the earlier stages of demixing, the rates for the 1:4 mixtures are generally greater than those for the 4:1 mixtures, suggesting that partial vacancies play an important role in the early-stage kinetics. An asymmetry in the domain sizes of the two components is found in the 1:1 mixtures, especially in the $C_{28}{}^H/C_{36}{}^D$ mixture. This asymmetry indicates that the domains of the longer chains are more compact than those of the shorter chains.

I. Introduction

Certain binary *n*-alkane solid solutions prepared by rapid quenching undergo spontaneous segregation at room temperature. After the quench, the time that must elapse before segregation can be detected ranges from a fraction of a second to years, depending on the average chain length of the two components and, more importantly, on the chain-length difference between the components. For some systems, the rate of segregation is such that it is possible to use conventional vibrational spectroscopy to monitor the demixing and to determine at the molecular level the nature of the process whereby the mixture goes from a solid solution to a partially segregated solid. The process is especially interesting for the binary *n*-alkanes because, in contrast to other chain systems in which microphase separation has been studied, the demixing takes place in a highly crystalline, anisotropic solid and involves some (small) degree of conformational ordering.

The phenomenon of microphase separation in binary *n*-alkane mixtures was first reported by Mazee[1] in a 1958 paper on an X-ray diffraction study of the $C_{30}{}^H/C_{35}{}^H$ (n-$C_{30}H_{62}/n$-$C_{35}H_{72}$) mixture. Mazee found that freshly melt-crystallized $C_{30}{}^H/C_{35}{}^H$ was initially a solid solution, but after a number of months had undergone some demixing. He speculated on the possibility that during the demixing process the solid might tend to form a "superlattice" structure in which layers of one phase would stack in a regular way with layers of the other phase. Subsequent to Mazee's paper the subject of microphase separation in *n*-alkane mixtures received little attention until Dorset[2,3] recently reported, from studies which employed differential scanning calorimetry (DSC) and electron diffraction, that the phenomenon is rather general, occurring in any number of binary *n*-alkane systems. This was followed by a very preliminary account[4] of the present results and by a small-angle neutron scattering study of demixing in a $C_{30}{}^H/C_{36}{}^D$ mixture.[5]

We report here on the measurement of the kinetics of microphase demixing in the binary mixtures C_{28}/C_{36}, C_{29}/C_{36}, and C_{30}/C_{36} at room temperature and at concentration ratios of 4:1, 1:1, and 1:4. First, the infrared method used to monitor the segregation is described, followed by a characterization of the kinetics. Then the dependence of the segregation rates on the chain-length difference and on concentration is considered.

This report focuses primarily on the kinetics of demixing. Other aspects of the demixing process, which include conformational ordering, crystal structure changes, and the dependency of the demixing rates on temperature, pressure, and isotopic composition, will be reported elsewhere.

II. Methods

A. Measurement of Infrared Spectra. The hydrogenated *n*-alkanes used (n-$C_{28}H_{58}$, n-$C_{29}H_{60}$, and n-$C_{30}H_{62}$) were of high purity (>99.5%) and are described in ref 6. The deuterated *n*-alkanes (n-$C_{30}D_{62}$ and n-$C_{36}D_{74}$) were purchased from MDS Isotopes. The manufacturer's specifications indicate a deuterium concentration of >99.0 atom %.

Thin films of the binary mixtures suitable for infrared transmission were prepared in a standardized manner. A weighed mixture of the *n*-alkanes was melted and stirred at 80 °C and cooled to room temperature. To make a film, approximately 25 mg of the solid mixture was placed on the surface of a horizontally-held KBr window, which was then heated until the solid melted. The mixture in the liquid state was maintained on the window for at least 10 min, after which a second window, at room temperature, was then placed over it. The resulting sandwich was then cooled to the desired temperature, normally 23 ± 1 °C, for the infrared measurements.

For measurements above or below room temperature, the freshly prepared sample was inserted into a thermostated copper holder. The temperature of the sample was maintained constant to within 0.2 deg of the desired value. The holder assembly, described in ref 7, uses a Neslab refrigerator bath to circulate water in the coils that surround the sample holder. To eliminate the problem of moisture condensation during measurements at low temperature, dry air was blown over the sample.

Infrared spectra were measured with an evacuated Nicolet Model 8000 FT IR spectrometer with a cooled MCT/InSb detector. The spectra were recorded with a resolution of 2 cm^{-1}. The time required to measure one spectrum was of the order of 5 min.

B. Determination of Domain Size. 1. Basis of the Method. Chain segregation in crystallne $C_n{}^H/C_{36}{}^D$ mixtures was followed

† Present address: Department of Chemistry, University of Toronto, Toronto, Ontario M5S 1A1, Canada.

0022-3654/92/2096-10008$03.00/0

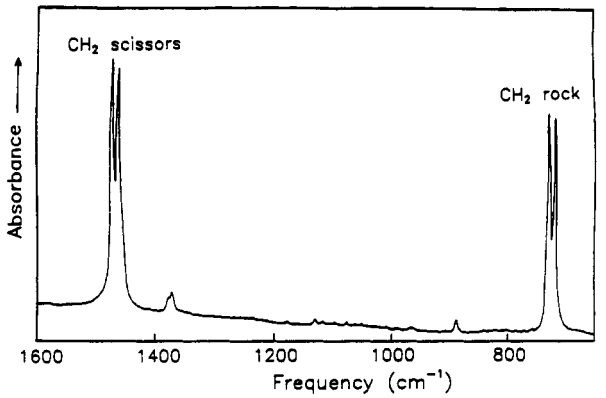

Figure 1. Infrared spectrum of crystalline n-$C_{60}H_{122}$ (22 °C) showing the splitting of the methylene scissors and rocking bands.

by monitoring the intermolecular splitting of the methylene-scissors band in the infrared spectrum. The degree of segregation is expressed in terms of N, the average number of chains in the domains (or clusters) of the component that was measured, usually the minority component in a mixture unbalanced in concentration.

The value of N can be estimated from the frequency separation between the scissors bands in the spectrum of a mixture of hydrogenated and deuterated n-alkanes. The method depends on the fact that the intermolecular coupling produces splitting only in the spectra of isotopically-alike chains; if the chains are isotopically different, the coupling is negligible and the spectrum is not affected. As a consequence, clusters of like chains are in effect vibrationally isolated from the surrounding chains. The frequency separation of the components increases with the size of the domain, and a quantitative relation between band separation and domain size can be derived on the basis of the simple model described below. The general technique of isotopic isolation method was first reported by Hiebert and Hornig.[8] It has since been widely used to study molecular clustering and to determine structure and intermolecular forces. It has also been applied to polymers, especially to investigate chain folding in semicrystalline polyethylene.[9]

The interchain band splitting is greatest for the pure n-alkanes. The splittings in the mixtures are measured relative to this maximum value. As may be seen in Figure 1 for $C_{60}H_{122}$, the intense bands near 1468 and 720 cm^{-1} are both split. These bands represent methylene-scissors and methylene-rocking fundamentals, respectively. The infrared spectra of the hydrogenated n-alkanes used in the present work are very similar to the spectrum shown in Figure 1. The corresponding bands for the deuterated n-alkanes occur near 1088 and 525 cm^{-1} and are similarly split. The scissors and rocking bands are both intense, so that either could be used to estimate domain size. We have used the scissors band because it occurs at an experimentally convenient frequency for both the hydrogenated and deuterated chains.

The interchain interaction that gives rise to the splitting is known to be short range.[10] This fact makes it possible to derive a simple relation between splitting and domain size. The force constants that couple the chains are associated primarily with short range H–H (or D–D) atom repulsion. The two bands produced by the coupling can be identified with the in-phase and out-of-phase vibrations of the two chains in the unit subcell.

2. The Relation between the Normalized Splitting and the Domain Size. It is convenient to convert the observed splitting to a normalized splitting, R, that is defined

$$R = \Delta\nu/\Delta\nu_0 \tag{1}$$

where $\Delta\nu$ is the splitting of the scissors band of either the hydrogenated or the deuterated n-alkane component and $\Delta\nu_0$ is the splitting for the neat n-alkane of the corresponding isotope. The splittings observed for the 1467- and 1088-cm^{-1} bands are thus put on a common scale so that they can be compared directly.

To derive a quantitative relation between cluster size and normalized band splitting, we first consider a one-dimensional crystal. For such a crystal the relation between R and N can be

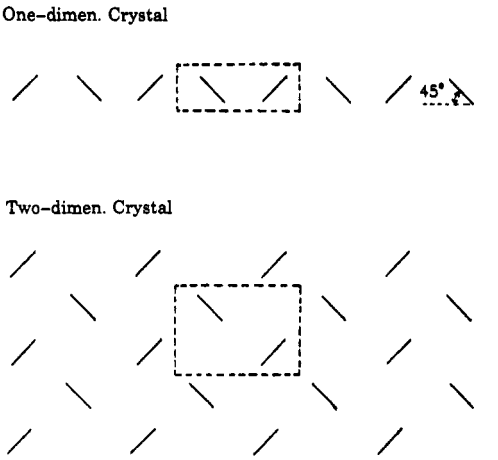

Figure 2. Structure of a one-dimensional and two-dimensional n-alkane crystal. Projection onto a plane perpendicular to the direction of the chains.

expressed by a simple equation, and this equation, with minor modification, applies in a good approximation to square-shaped, two-dimensional clusters. The one-dimensional crystal, which is depicted in Figure 2, consists of a row of N chains that are alternately oriented so as to correspond to the 110 plane in the orthorhombic crystal. The orthorhombic crystal is also depicted in Figure 2. We assume that the scissors mode of a given chain is intermolecularly coupled to its nearest-neighbor chains and that the intermolecular force constant connecting the scissors modes has the same value for both the one- and two-dimensional crystals.

The scissors band in the spectrum of the one-dimensional crystal consists of two equally intense components. One of these is the in-phase mode, which is polarized parallel to the crystal direction. This mode may be depicted

↗↘ ↗↘ ↗↘ ↗↘

where, as we look down the length of the chains, the arrows represent the dipole derivatives with respect to the scissors mode. The out-of-phase perpendicular mode may be similarly depicted

↗↖ ↗↖ ↗↖ ↗↖

The zone-center vibrational frequencies for the one-dimensional crystal are given by

$$\lambda_k = a + 2b \cos \frac{k\pi}{N+1} \tag{2}$$

where $\lambda_k = 4\pi^2c^2\nu_k^2$ and k is an integer that goes from 1 to N, c is the velocity of light, ν_k is the frequency in cm^{-1} of the kth mode, a and b are respectively diagonal and off-diagonal matrix elements connecting the intrachain vibrations, and N is the number of chains in the crystal. The infrared allowed vibrations are $k = 1$ and $k = N$. The relative frequency separation between the (in-phase and out-of-phase) vibrations is then

$$R = \cos \frac{\pi}{N+1} \tag{3}$$

where R is the normalized splitting defined in eq 1. For the infinitely long one-dimensional crystal, the splitting in terms of λ_k is $\Delta\lambda_k = 4b$. The relative intensities of the two component bands depend on the angle between the skeletal plane of the n-alkanes and the direction of the one-dimensional crystal, as shown in Figure 2. The corresponding angle in the (two-dimensional) orthorhombic crystal has been experimentally determined to be about 45°,[11] and we assumed this value. For this value the intensities of the component bands are equal to each other, for both the one- and two-dimensional crystals. Finally we note that for the one-dimensional crystal eq 3 may be expressed in the form

$$N = \frac{\pi}{\sqrt{2(1-R)}} - 1 \tag{4}$$

in which case N is easily calculated. This form of the equation is quite accurate for $N \geq 3$.

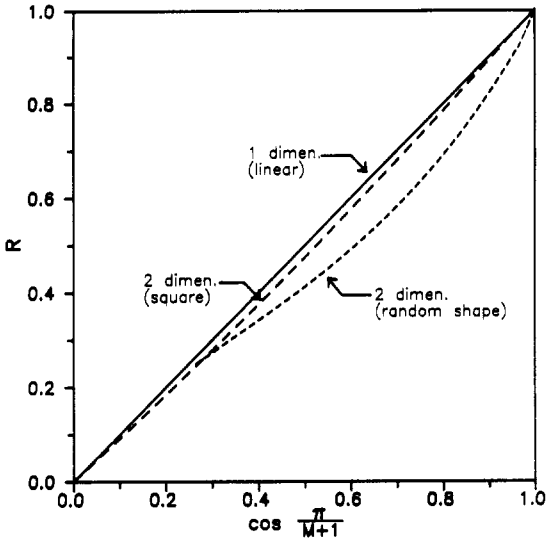

Figure 3. The normalized splitting, R, of the scissors band plotted against cos $[\pi/(M + 1)]$ for a one-dimensional lattice of chains and for two two-dimensional lattices (square shapes and random shapes). For the one-dimensional case, $M = N$, and for the two dimensional case, $M = N^{1/2}$, where in both cases N is the number of chains in the domain.

The relation between R and N for the two-dimensional crystal was determined numerically. In the two-dimensional crystal, a chain can interact with its four nearest neighboring chains (Figure 2). For this interaction to occur, however, the neighboring chains must be isotopically identical. In two dimensions, there is a complication in that the degree of splitting associated with a domain of a given number of chains is dependent on the shape of the domain. We have considered two situations: (i) all domains are square; (ii) each domain has a random shape.

The normalized splitting associated with square domains, which we will take to represent "compact" domains, was found to a good approximation to be given by the expression

$$R = \cos \frac{\pi}{N^{1/2} + 1} \tag{5}$$

The observed splitting for the infinite two-dimensional crystal is then $\Delta\lambda_k = 8b$, twice that for the one-dimensional crystal. This equation is like eq 3 except that N has been replaced by $N^{1/2}$.

For the random case, the splitting was obtained from the calculated spectra of large ensembles of randomly shaped domains. Each domain was generated by adding one chain at a time to the edge of a domain consisting initially of a single chain. The placement of each additional chain was random; that is, the probability for addition was equal for all edge sites. After the domain had grown to a total of N chains, the process was stopped. The calculated values of the normalized splitting, R, for linear, square, and randomly-shaped domains are shown in Figure 3 as a function of the phase angle defined in the caption.

The calibration curve used to determine domain size from observed splitting is shown in Figure 4. This curve is the average of the curves for the square and random-shaped domains. These latter curves, also shown in Figure 4, are similar if N is small but diverge significantly for large N. The calibration curve was taken as the average of these because it was assumed that "surface tension" effects would tend to smooth the contours of the domains and thus, on the average, nudge the random shapes toward somewhat more compact forms.

It is appropriate then to emphasize that, while the magnitude of the splitting reflects mainly the average size of domains, it could be affected by domain shape. As indiciated in Figure 4, for a constant value of N the splitting increases as the domains become more compact. We have assumed that the domains of the minority component will tend to have relatively uniform, compact shapes, and therefore the splitting will give a good measure of their average size. This assumption becomes questionable if the concentrations of the components are comparable.

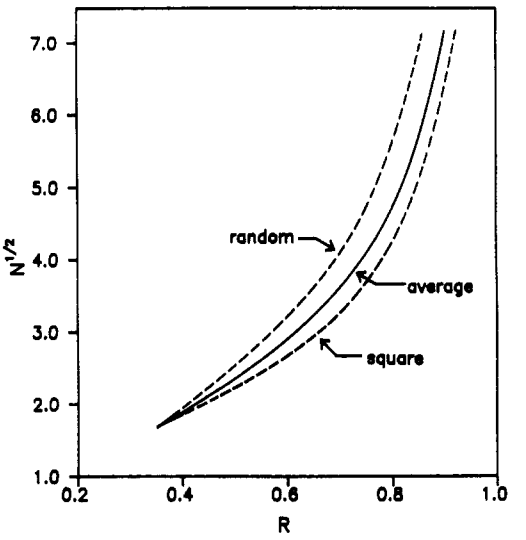

Figure 4. Calibration curves relating $N^{1/2}$, the root mean-square number of chains making up a domain, and R, the normalized splitting of the scissors band. The curve used in this report is the average of the curves derived for the square and random-shape cases.

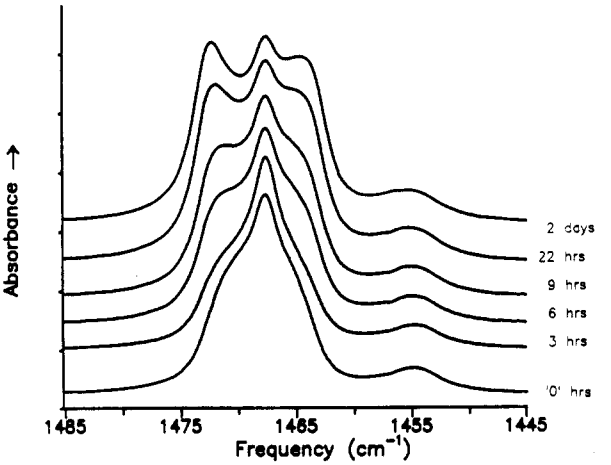

Figure 5. Example of the time evolution of the infrared scissors band of C_{30}^H during microphase segregation in the 1:4 mixture C_{30}^H/C_{36}^D at 22 °C.

In principle, the intensity of the central band can be used to estimate the concentration of isolated or nearly isolated chains. In practice, however, it is difficult to do this because the central band is badly overlapped with the component bands of the doublet and because the shape of the doublet is not quantitatively known. For mixtures studied here, there is a strong inverse relation between the degree of splitting (domain size) and the intensity of the central band that makes it possible to use domain size as a basis for comparing and characterizing different mixtures with an accuracy adequate for our purposes here.

C. Analysis of the Scissors Band Doublet. Spectra typical of a partially phase-separated mixture are shown in Figure 5. This series shows the time evolution of the CH_2 scissors band for a freshly prepared mixture C_{30}^H/C_{36}^D at a molar concentration ratio of 1:4. In the first spectrum the scissors band consists of an intense central component with low-intensity shoulders on both sides. The shoulders increase in intensity in each succeeding spectrum, doing so at the expense of the central band. All the spectra shown in this figure display the triplet pattern that characterize a partially segregated binary mixture.

The contour of the scissors band observed for a partially segregated mixture differs significantly from that observed for a mixture of the same composition in which the chains are randomly distributed. The scissors bands for random mixtures are approximated in Figure 6 by the scissors bands for the mixture C_{36}^H/C_{36}^D. The band associated with the minority component at low concentration is a singlet and remains one up to concen-

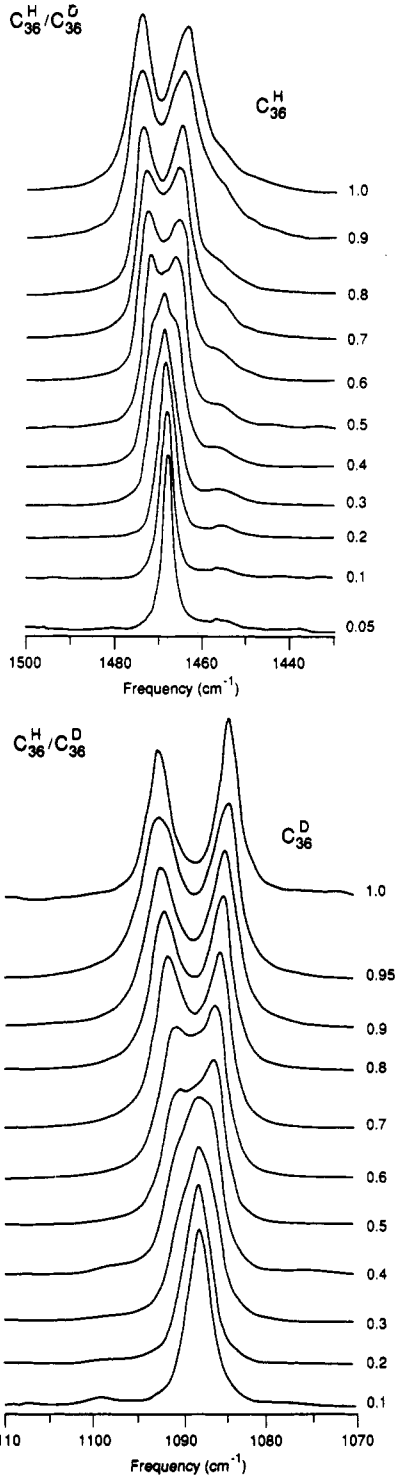

Figure 6. Infrared spectra of C_{36}^H/C_{36}^D mixtures at 22 °C in the CH_2 and CD_2 frequency regions. The mole fraction of the component observed is indicated.

trations around 50%. Above 50%, the band is a doublet. Only at concentrations very near 50% does the band resemble a triplet.

The assignment of the scissors triplet is spelled out in Figure 7 for a partially segregated C_{30}^H/C_{36}^D 1:4 mixture. The two outside bands are associated with the domains of the minor component, that is, with C_{30}^H-rich domains. The average size of these domains can be established from the frequency separation of the outer bands. The majority-component C_{36}^D chains that are isolated in the C_{30}^H domains contribute in the CD_2-scissors frequency region to a band centered between the components of the CD_2 doublet, near 1088 cm^{-1}. (This spectral region is not shown.) The central band in Figure 7 is associated with the C_{30}^H chains that are isolated in the matrix consisting of the C_{36}^D majority component.

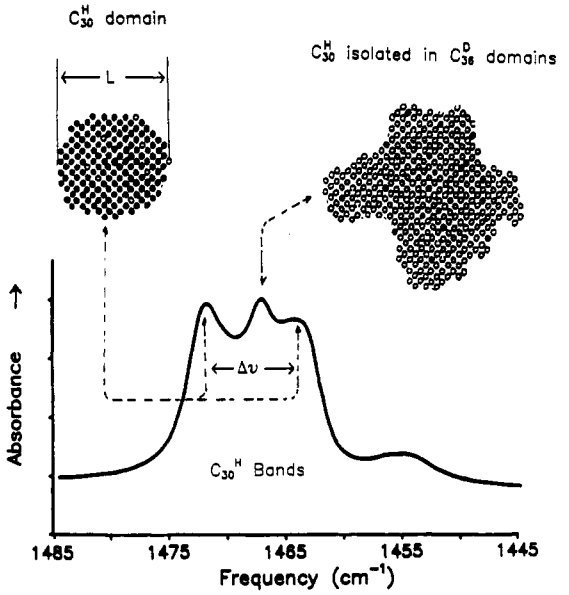

Figure 7. Assignment of the three components of the infrared CH_2 scissors band in a partially segregated C_{30}^H/C_{36}^D mixture.

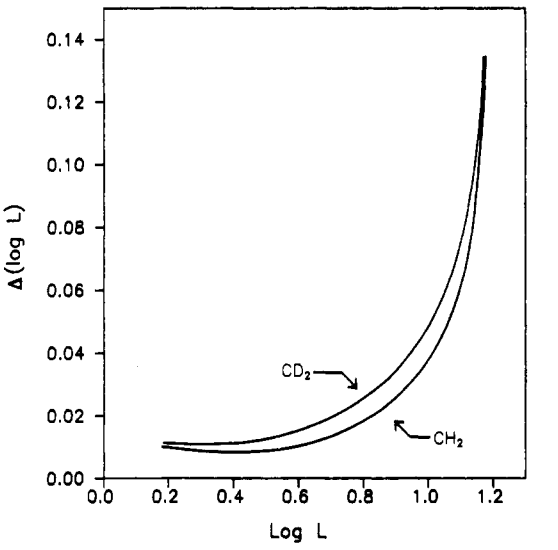

Figure 8. Estimated change in log L that results from a change of 0.1 cm^{-1} in the splitting of the scissors band, as a function of log L, where L is the average width of the domains ($L = N^{1/2}$).

To evaluate in a consistent way the value of the splitting, the components of the triplet were separated using the band-fitting option in the program SPECTRA CALC. We have assumed that the three bands have symmetric shapes, although both observed and calculated spectra indicate that the two outer bands are intrinsically asymmetric. The high-intensity side is in the region between the bands. As a consequence of having assumed that the outer bands are symmetric, the intensity of the middle band tends to be badly determined. The frequency separation between the outer bands is, however, well determined.

Errors in the estimated domain size arise from inaccuracies in the measured value of the splitting and also from uncertainties in the calibration curve. If R is near 1.0, these errors can greatly affect the estimated domain size. The errors in the measured splitting are of the order of ±0.1 cm^{-1}. Figure 8 indicates the change in the estimated domain size that results from a change of 0.1 cm^{-1} in the splitting. In this figure, the domain size is expressed as log L, where L is the average width of the domains in terms of number of chains.

D. The C_{36}^H/C_{36}^D Mixture as Reference for Randomness. The degree to which a binary system has demixed at the time of the first measurement after the quench can be estimated by comparing the shape of the scissors band with the corresponding band for

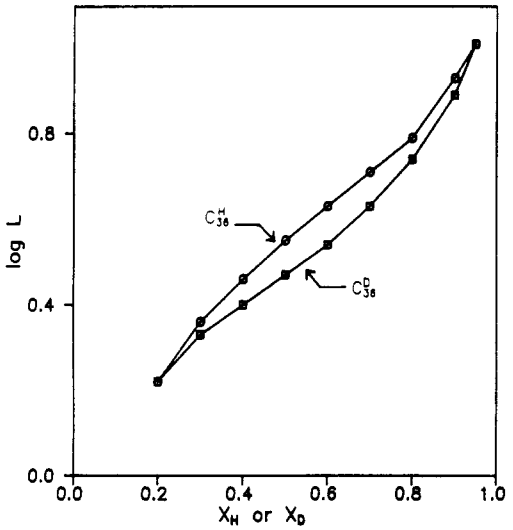

Figure 9. Average size of C_{36}^H and C_{36}^D domains in terms of log L for random mixtures, as a function of concentration. Based on the splitting of the infrared scissors band observed in the IR spectra of C_{36}^H/C_{36}^D mixtures.

a random mixture. As noted above, the scissors band for a random mixture is represented in good approximation by the spectrum of the solid solution C_{36}^H/C_{36}^D (Figure 6).

It is generally assumed that there is very little demixing in the binary mixture C_{36}^H/C_{36}^D. While theory[12] and experiment[13] both indicate randomness, the existence of a small degree of demixing cannot be ruled out. Our measurements, if taken at face value, indicate a small degree of segregation. This is evident from a comparison of the average sizes of the C_{36}^H and C_{36}^D domains, which were determined from the splitting in the C_{36}^H/C_{36}^D spectrum. These domain sizes are shown in Figure 9 as a function of composition.

The C_{36}^H domains appear to be slightly larger than those of C_{36}^D. The difference could be due to systematic errors in the estimation. However, we cannot rule out the possibility that the difference is real. Further measurements are being made to determine this.

It is informative to compare the experimentally estimated domain sizes for the C_{36}^H/C_{36}^D mixture with values estimated on the assumption of random mixing. One way to do this is to compare the value of L_i, the average width of the domains of the ith component in the mixture, with L_i', the average length of sequences of chains of the same component in the one-dimensional crystal. Given that the mole fraction of component i is X_i, the value of L_i' may be calculated from

$$L_i' = \frac{1 + X_i}{1 - X_i} \tag{6}$$

Equation 6 was derived from the equations given in ref 14. For 4:1 and 1:4 mixtures of C_{36}^H/C_{36}^D, we find from Figure 9 that the average value of L for the minority component is 1.7 while L', the calculated value for the one-dimensional crystal, is 1.5. Similarly for the 1:1 mixture, L and L' are respectively 3.2 and 3.0. By this criterion, the accuracy of the spectroscopically determined domain sizes appears to be quite good.

III. Results

A. Phase Behavior. Evidence for microphase separation in melt crystallized binary n-alkane mixtures has been reported by Dorset[2,3] from DSC (differential scanning calorimetry) measurements. DSC curves for C_{30}^H/C_{36}^D are shown in Figure 10. The upper curve is for a 1:1 mixture just after crystallization and the lower curve is for the same sample after it had aged for several days at room temperature. Both curves show two prominent endotherms, one associated with the solid–solid orthorhombic to hexagonal phase transition and the other with the hexagonal to liquid transition. However, the DSC curve of the aged sample shows an additional endotherm near 50 °C that is not present for

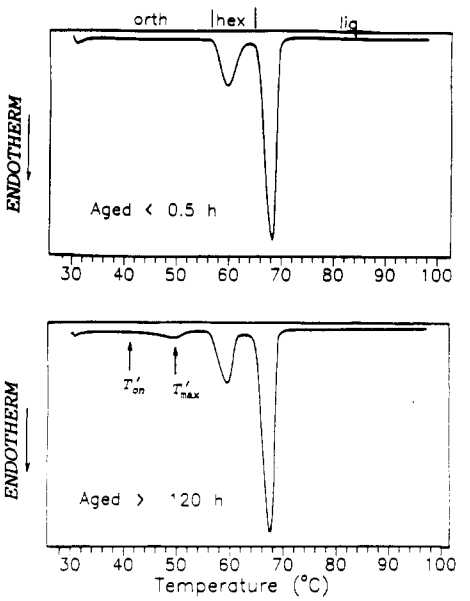

Figure 10. DSC curve of a 1:1 C_{30}^H/C_{36}^D melt-crystallized mixture. Top: the curve measured within 0.5 h of the crystallization. Bottom: the curve measured after the sample was aged in excess of 120 h. T_{on}' marks the onset temperature of the "mixing" endotherm and T_{max}' marks the temperature the maximum.

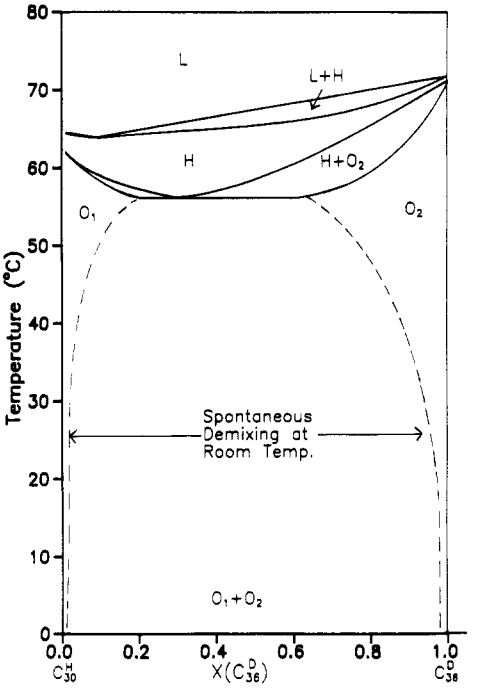

Figure 11. Approximate phase diagram of the binary mixture C_{30}^H/C_{36}^D based on DSC measurements. L, liquid; H, hexagonal crystal; O_1, orthorhombic crystal rich in C_{30}^H; O_2, orthorhombic crystal rich in C_{36}^D. The shape of the coexistence curve, indicated by the dashed line, is uncertain, especially at temperatures below 50 °C.

the freshly prepared sample. The new endotherm is present in all the DSC curves of aged C_{30}^H/C_{36}^D mixtures having a C_{36}^D mole fraction concentration in the approximate range 0.1–0.9. This endotherm is associated with the microphase mixing of the partially segregated mixture.[2,3]

The demixing observed in the present study occurs entirely in the orthorhombic phase. This follows from the phase diagram that we have constructed from DSC curves of mixtures at various concentration ratios. The phase diagram for C_{30}^H/C_{36}^D (Figure 11), which is similar to that determined by Mazee[1] for C_{30}^H/C_{35}^H, indicates that at room temperature the n-alkane mixtures have orthorhombic crystal structures that are well removed in temperature from the hexagonal structure. However, it is important

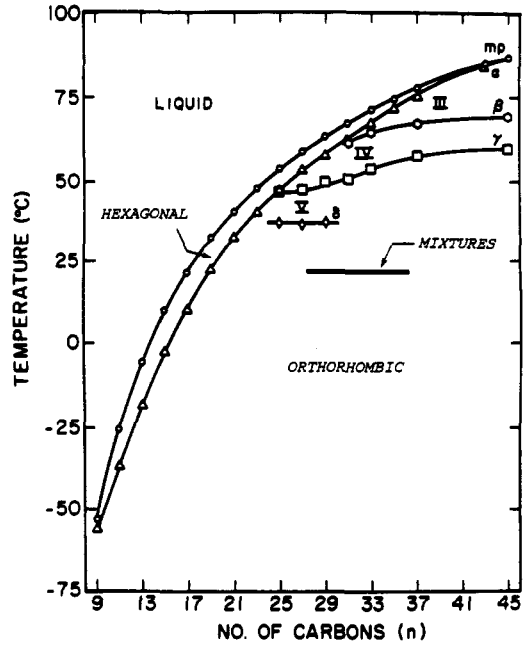

Figure 12. "Phase diagram" for the odd-numbered *n*-alkanes. The chain length region of the *n*-alkanes that make up the binary mixtures in the present study is shown and the liquid and hexagonal regions are marked. The other crystalline phases have orthorhombic-subcell structures.

to note that, while the unit subcell is always orthorhombic, there are several types of crystal structures in this temperature region. Some of these are discussed in ref 15 for the pure *n*-alkanes and in refs 3 and 16 for the mixtures. Figure 12 shows a "phase diagram" for the neat *n*-alkanes[17] on which is marked the chain-length region that takes in the *n*-alkanes making up the binary mixtures studied here. Some of the variants of the orthorhombic subcell structures are indicated on this figure.

A binary solid solution is indefinitely stable if the chain-length difference is only a few carbons, the exact number depending to some extent on the average chain length of the two components. The mixtures C_{19}/C_{21} and C_{46}/C_{50}, for example, form stable solid solutions. (The conformational disorder in these solid solutions has been a subject of our earlier studies[6,7]).

The immiscibility of the *n*-alkane components increases with the chain-length difference. The minimum value of the difference required for phase separation has been considered in two recent papers. Matheson and Smith[18] presented a map indicating which binary *n*-alkane mixtures are stable and which are not. More recently, Dorset[3] reported a more extensive set of data, which is summarized in Figure 13. The binary mixtures of interest (C_{28}^H/C_{36}^D, C_{29}^H/C_{36}^D, and C_{30}^H/C_{36}^D) are marked on the figure.

B. Measurements of C_n^H/C_{36}^D 4:1 and 1:4 Mixtures for n = 28, 29, and 30. The spectra of the 4:1 mixtures in the CD_2-scissors band region of the minority C_{36}^D component are shown in Figure 14 as a function of time. The CD_2 scissors band evolves in a similar manner for each mixture. The two outside bands, which are associated with domains consisting of two or more C_{36}^D chains, increase in intensity while the frequency separation between them also increases. The rate of demixing is, however, clearly very different for the different mixtures.

1. The Initial Measurements after Quenching. Our spectra show that a measurable amount of phase separation occurs in the time interval between the quench and the measurement of the first spectrum, which will be referred to as the time-zero spectrum. Some demixing occurs both during the quench, which requires perhaps 2 min (the time needed for the sample to return to room temperature) and during the measurement of the first (time-zero) spectrum, which requires about 4 min. Consequently our estimates of the (effective) elapsed time that is to be associated with the time-zero spectra are highly uncertain. The values chosen are generally somewhere around 5 min.

The demixing rate for the C_{30}^H/C_{36}^D 4:1 mixture is among the slowest of the mixtures considered here. Nevertheless, some

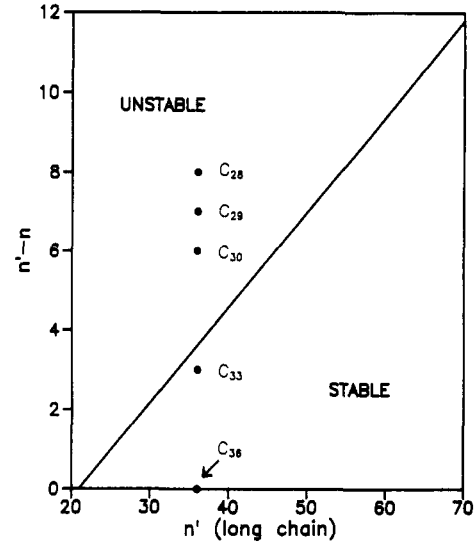

Figure 13. Map showing regions of stable and unstable binary *n*-alkane solid mixtures $C_n^H/C_{n'}^H$. Based on data from ref 3.

time-zero demixing occurs. This is evidenced by a broadening of the CD_2 band due to some degree of splitting. The broadening is apparent from a comparison of the width of the CD_2 band with that of the corresponding band in the spectrum of the 4:1 C_{36}^H/C_{36}^D mixture, which represents the random case. Time-zero demixing for the 4:1 C_{28}^H/C_{36}^D mixture is, on the other hand, much greater as is obvious from the degree of C_{36}^D-band splitting indicated in Figure 14.

Mixtures that demix very quickly, such as C_{28}^H/C_{36}^D, probably do so largely during the quenching period, since demixing can proceed more rapidly above room temperature. Our measurements on the temperature dependence of segregation indicate this. For example, as a C_{30}^H/C_{36}^D mixture is cooled from the temperature (about 50 °C) at which it is a solid solution, it begins to demix near 45 °C, and between 45 and 30 °C the rate of demixing reaches a maximum that is significantly greater than the room-temperature rate.[19]

2. Segregation Behavior with Time: log L versus log t Plots. The segregation kinetics can be displayed in several ways. In Figure 15, the observed splitting frequency of the CD_2 scissors band for the 4:1 C_{30}^H/C_{36}^D mixture is plotted against time. The increase in splitting slows with time so that the splitting appears to be approaching a constant value at very long times. Therefore, we attempted to fit the observed splitting using an exponential function of the type $a + be^{-ct}$, where t is time and a, b, and c are parameters whose values might be evaluated from the experimental data. The parameter c would then serve as a basis for comparing different mixtures. However, it was found that the time dependence of the splitting is not well represented by this function.

A plot that relates the average number of chains in a C_{36}^D domain to the time elapsed after quenching is shown in Figure 16 for the 4:1 mixtures C_{28}^H/C_{36}^D and C_{30}^H/C_{36}^D. The plot shows that the C_{36}^D clusters are small for these mixtures. For C_{30}^H/C_{36}^D, the C_{36}^D clusters contain 7–9 chains at time-zero. After about 70 h, they still average only about 28 chains. In the case of the faster segregating C_{28}^H/C_{36}^D mixture, the C_{36}^D clusters consist initially of about 26 chains, increasing in size to about 70 chains after 50 h.

One convenient and informative way to display the time dependence of segregation is in terms of log L versus log t, where L is the average lateral dimension of the minority-component domains and t is the time elapsed after quenching. The value of L is taken to equal $N^{1/2}$. The basis for the use of log/log plots is that power-law relations of the form

$$P = Kt^{\alpha} \tag{7}$$

which connect a certain property P with time t have been shown from both theory and experiment to describe the demixing dynamics in quenched systems.[20] Typically, P is the average con-

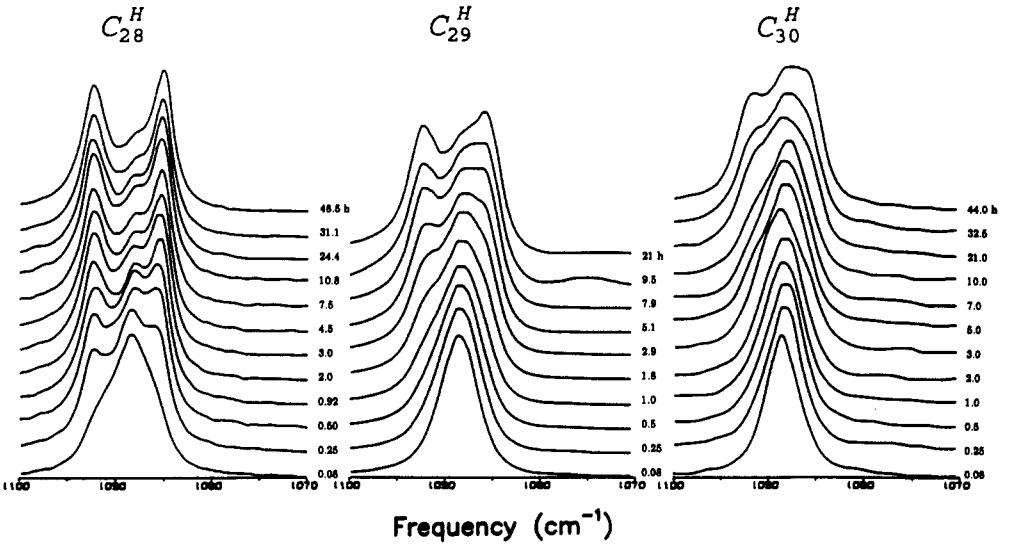

Figure 14. Infrared spectra for the 4:1 mixtures C_{28}^H/C_{36}^D, C_{29}^H/C_{36}^D, and C_{30}^H/C_{36}^D at room temperature, as a function of elapsed time after the quench.

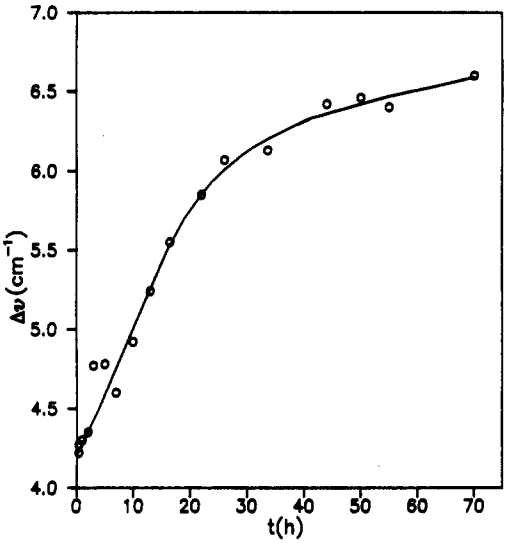

Figure 15. Splitting of the scissors band of C_{36}^D as a function of time for the C_{30}^H/C_{36}^D 4:1 mixture at room temperature.

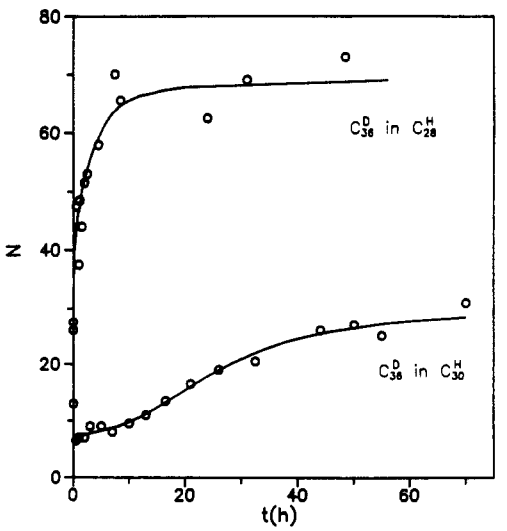

Figure 16. Average C_{36}^D domain size in terms of number of chains plotted as a function of time for 4:1 mixtures C_{28}^H/C_{36}^D and C_{30}^H/C_{36}^D at room temperature.

centration correlation length or the maximum intensity derived from light or X-ray scattering measurements.[21,22] There exists a large literature on the theoretical evaluation of the exponential

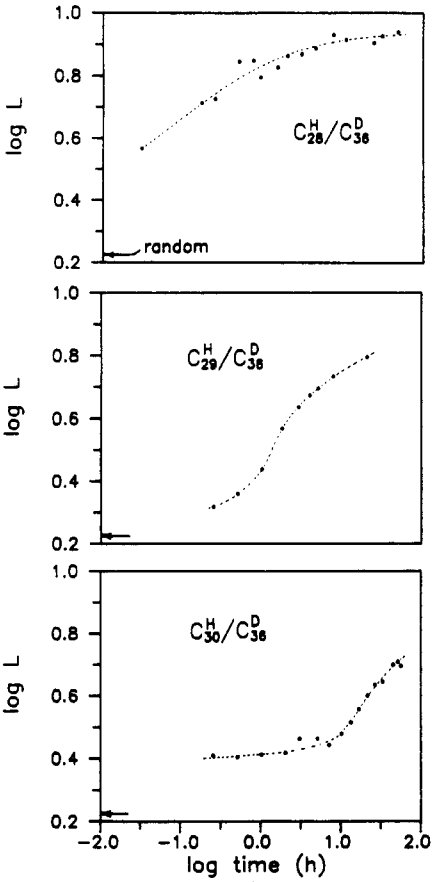

Figure 17. log L plotted against log t for the 4:1 mixtures C_{28}^H/C_{36}^D, C_{29}^H/C_{36}^D, and C_{30}^H/C_{36}^D at room temperature. The estimated value of log L (= 0.22) for random mixing is marked on each plot.

α, based on more or less simple model systems. It appears, however, that none of the models so far treated relate directly to the present systems.

Figure 17 shows log L versus log t plots for the 4:1 mixtures C_{28}^H/C_{36}^D, C_{29}^H/C_{36}^D, and C_{30}^H/C_{36}^D, and Figure 18 shows same kind of plots for the corresponding 1:4 mixtures. The values of log L associated with random mixing (evaluated from the C_{36}^H/C_{36}^D mixture) are indicated on these figures.

It is important to note that the log/log plots we observe are not at all linear but have complex shapes and, moreover, shapes that change in going from one mixture to another. However, the changes in shape are systematically related to the chain lengths of the n-alkane components as follows. The curve representing

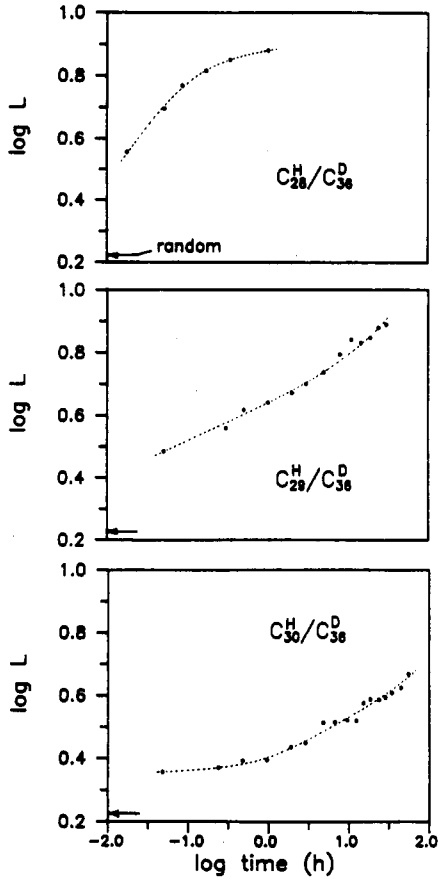

Figure 18. log L plotted against log t for the 1:4 mixtures C_{28}^H/C_{36}^D, C_{29}^H/C_{36}^D, and C_{30}^H/C_{36}^D at room temperature. The estimated value of log L (= 0.22) for random mixing is marked on each plot.

the C_{36}^D clusters in the C_{30}^H/C_{36}^D 4:1 mixture remains nearly flat for about 10 h, after which it undergoes a turn upward. At very long times there is a slight tendency to level off. The same curve for the intermediate mixture, C_{29}^H/C_{36}^D, first turns upward and then levels off. For the last mixture in the series, C_{28}^H/C_{36}^D, the curve is initially steep, but then appears to level off. The log/log plots of the 1:4 series and, as will be seen later, the 1:1 series show similar, though somewhat less well defined, behavior.

These observations suggest that the individual log/log curves for a given concentration ratio may represent, if properly scaled in time, different regions of a common log/log curve. Figure 19 shows the approximate shapes of the common curves for the minority component in the 4:1 and 1:4 mixtures. These curves were constructed by combining, with some minor adjustments, the 3 log/log plots shown in Figure 17 for 4:1 and in Figure 18 for 1:4. The common curves were obtained by translating along the log t axis the plots of the C_{29}^H/C_{36}^D and C_{28}^H/C_{36}^D mixtures so as to produce a more or less continuous curve. The approximate time span (beginning and ending times: 0.3 and 31.5 h after the quench), over which the actual measurements were carried out, are indicated on Figure 19 for each mixture. The translation along the log t axis is equivalent to multiplying the time scale for each mixture by a constant factor. The multiplication factors are 1, 6, and 600 for the minority components (C_{30}^H, C_{29}^H, and C_{28}^H, respectively) in the 4:1 mixtures and are 1, 63, and 3400 for the C_{36}^D minority component in the corresponding 1:4 mixtures. The multiplication factor is an approximate measure of the rate of demixing relative to C_{30}^H/C_{36}^D.

The common curves are useful for characterizing the general features of the kinetics and specifically for comparing the 4:1 and 1:4 mixtures. The curves shown in Figure 19 for these two mixtures are similar; both are S-shaped. There is a region of upward curvature that occurs soon after the quench, which we have designated as the π-break, although this so-called "break" is usually not very sharp. This is followed by an inflection region of maximum slope that tends to be linear. Finally, there is a

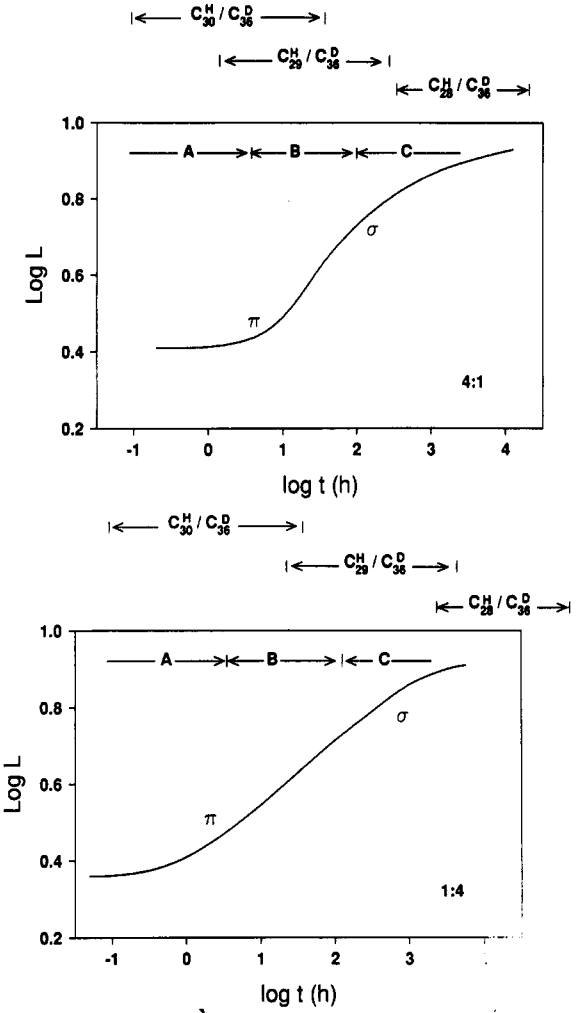

Figure 19. "Common" log L vs log t curves constructed from the log L vs log t plots indicated in Figures 17 and 18 for the three binary mixtures having 4:1 and 1:4 composition ratios. The approximate regions of log t that were actually measured are indicated for each mixture (see text).

leveling off at the longest times. We have designated the beginning of the leveling off as the σ-break, a break that is never sharp. The π- and σ-breaks, so defined, serve to divide the common plot into three regions, designated A, B, and C, as indicated on Figure 19.

Overall the common curves for the 4:1 and 1:4 mixtures are similar in shape, with the limiting domain sizes ($t = \infty$) being similar. The main difference between the two curves is in the π-break, which, for the 4:1 mixture, tends to be much sharper and to occur at a later time. A possible explanation for these differences will be considered below.

3. Dependence of the Segregation Rate on the Chain-Length Difference and on the Concentration Ratio. As already noted, the scale factors needed to adjust the time coordinate in constructing the common curves indicate that the segregation rate for both the 4:1 and 1:4 mixtures increases dramatically as the chain-length difference between the components increases. We will estimate this dependence in a more accurate way using the ratio of the segregation rates, r_1 and r_2, corresponding to mixtures 1 and 2. This ratio, defined $V = r_1/r_2$, is more or less dependent on the domain size L (or equivalently, on the time elapsed after the quench). V is determined from the ratio t_2/t_1, where t_1 and t_2 are the times required for the domains in the two mixtures to reach the same average size, L.

The dependence of the rates on the chain-length difference is shown in Figure 20 in terms of the log of the rate ratios, $r(C_{28}^H/C_{36}^D)/r(C_{30}^H/C_{36}^D)$ and $r(C_{29}^H/C_{36}^D)/r(C_{30}^H/C_{36}^D)$, which are plotted against log L for the minority components for both the 4:1 and 1:4 mixtures. The rate ratios are determined are mostly in range of log L from 0.55 to 0.75. Although the relative rates vary somewhat with L, they are clearly very different for

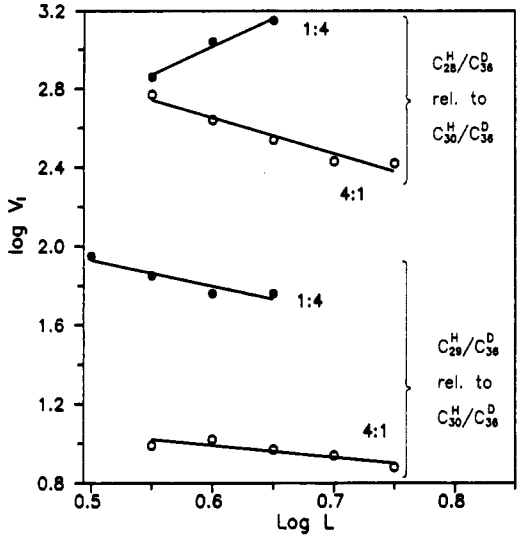

Figure 20. Dependence of the rate of demixing upon chain length: In terms of log V_1 as a function of L, where V_1 is equal to the rate ratio $r(C_{28}^H/C_{36}^D)/r(C_{30}^H/C_{36}^D)$ or $r(C_{29}^H/C_{36}^D)/r(C_{30}^H/C_{36}^D)$ (see text).

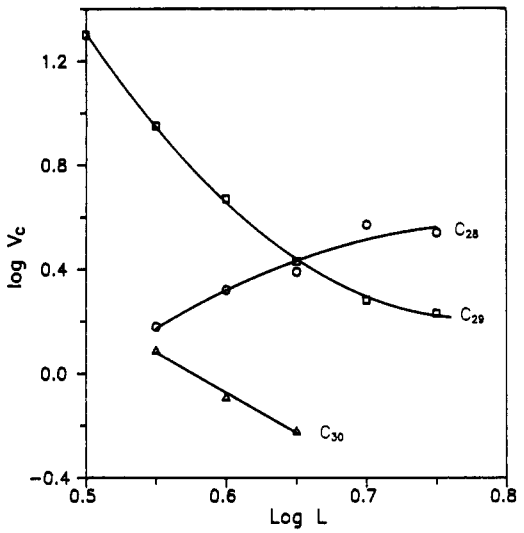

Figure 21. Dependence of the rate of demixing upon concentration: In terms of log V_c as a function of L, where V_c is equal to the rate ratio $r(1:4)/r(4:1)$. Estimated error in log V_c is about 0.2 (see text).

different mixtures, increasing dramatically with the chain-length difference for both sets of mixtures. The dependence is stronger for the 1:4 mixture.

The demixing rates of the 1:4 mixture relative to that for the 4:1 mixture have also been determined. Again, the ratios are based on the minority component and determined in the range of log L from about 0.55 to 0.75. The log of the rate ratios are plotted in Figure 21 as a function of log L. For C_{28}^H/C_{36}^D and C_{29}^H/C_{36}^D, the 1:4 mixtures segregate significantly faster than the corresponding 4:1 mixtures. For C_{30}^H/C_{36}^D, the rates are comparable.

C. Measurements on C_n^H/C_{36}^D 1:1 Mixtures with n = 28, 29, and 30. The log L versus log t plots for the 1:1 mixtures are shown in Figure 22. The domains in the 1:1 mixture are, of course, larger than those for the minority component in the 4:1 and 1:4 mixtures. The domains in the 1:1 mixtures, measured just after the quench, are also significantly larger than in the corresponding random mixture. As expected, time-zero demixing increases in going from C_{30}^H/C_{36}^D to C_{29}^H/C_{36}^D to C_{28}^H/C_{36}^D.

The shapes of the log L vs log t curves for the 1:1 mixtures are similar to those observed for the 4:1 and 1:4 mixtures except, as already noted, domain sizes are larger for the 1:1 mixtures. The curves for the 1:1 mixture also appear to represent segments of a common curve. However, relative to the curves for 4:1 and 1:4 mixtures, the 1:1 curves show less tendency to level off. After 100 h, the curves for the 1:1 mixtures have not leveled off in any degree comparable to the 4:1 and 1:4 mixtures.

For the C_{36}^D domains in the 1:1 C_{28}^H/C_{36}^D mixture, it should be mentioned that the accuracy in determining domain size after prolonged aging is relatively low because the observed value of R is near 1.0.

Because the 1:1 mixtures are compositionally symmetric, it is of interest to compare the values of the domain sizes measured for the two components. It is found that these values of L differ for all three mixtures. In each mixture the domains of the longer (deuterated) chains appear to be larger than those of the shorter (hydrogenated) chains. The difference is smallest for the C_{30}^H/C_{36}^D and C_{29}^H/C_{36}^D mixtures, amounting to about 0.05–0.08 units of log L, and is opposite that observed for the 1:1 "random" C_{36}^H/C_{36}^D mixture. For the latter mixture, the domains of *hydrogenated* chains appear to be the larger, by about 0.08 units of log L. (See Section II.D.) Consequently, the possibility that the apparent size difference observed for the mixture is due to an inaccurate calibration curve seems to be ruled out. If the calibration curve were "corrected" so that the sizes of the domains of C_{36}^H and C_{36}^D were made equal for the C_{36}^H/C_{36}^D mixture, the use of the new calibration curve would result in an *increase* the domain-size differences in both the C_{30}^H/C_{36}^D and C_{29}^H/C_{36}^D mixtures.

For the C_{28}^H/C_{36}^D 1:1 mixture, the apparent domain-size difference is much larger than for C_{30}^H/C_{36}^D or C_{29}^H/C_{36}^D and is certainly much too large to be attributed to an inaccurate calibration curve. The C_{36}^D domains are larger than those of C_{28}^H by 0.27–0.32 units of log L. This is the case starting immediately after the quench and continuing till the end of the measurements. The significance of this observation will be discussed below.

IV. Discussion and Summary

Crystalline solid solutions of C_{28}^H/C_{36}^D, C_{29}^H/C_{36}^D, and C_{30}^H/C_{36}^D were prepared by rapid quenching. The demixing kinetics were monitored using the interchain splitting of the infrared methylene-scissors band, from which the average domain size of the separate component phases were estimated. The infrared measurements were commenced shortly after the quench was completed and were continued for periods up to 4 days. For the 4:1 and 1:4 mixtures, only the minor component was monitored; for the 1:1 mixture, both components were included. The domains monitored varied in size from single chains to aggregates of several hundred chains.

A. Characterization of the Kinetics: log L vs log t Plots. The time evolution of the demixing kinetics is similar for all mixtures. This is evident if the kinetics of demixing are displayed in terms of log L versus log t plots, where L is an average linear dimension of the domain size ($L = N^{1/2}$) and t is the time. The log/log plots in Figures 17, 18, and 22 are assumed to represent different segments of a common (S-shaped) curve. Common curves constructed for the 4:1 and 1:4 mixtures are shown in Figure 19. These show two breaks where the demixing rates begin to undergo changes. The breaks are labeled π and σ.

The π-break occurs not long after the quench. It is seen most clearly for mixtures in which the longer chain, C_{36}, is the minority component. This break probably is the result of a structural transition in which there is an increase in the conformational ordering in the interlayer region. The transition might commence when the domains made up of the longer chains have become large enough to stabilize the constituent chains in their all-trans conformation. Earlier studies have shown that the long chains, which are diluted in solid crystalline solution of short chains, have ends that are likely to be conformationally disordered.[6] As the concentration of the long chains is increased, the disorder rapidly diminishes because the long chains are much more likely to assume all-trans conformations as they aggregate. The conformational ordering will lead to a higher degree of crystallinity and will result in an increase in the number of well defined partial voids that, in turn, will increase the overall rate of demixing. More information on the nature of the π-break is obviously needed to test this hypothesis.[23]

The σ-break, which occurs late in the demixing process, is not

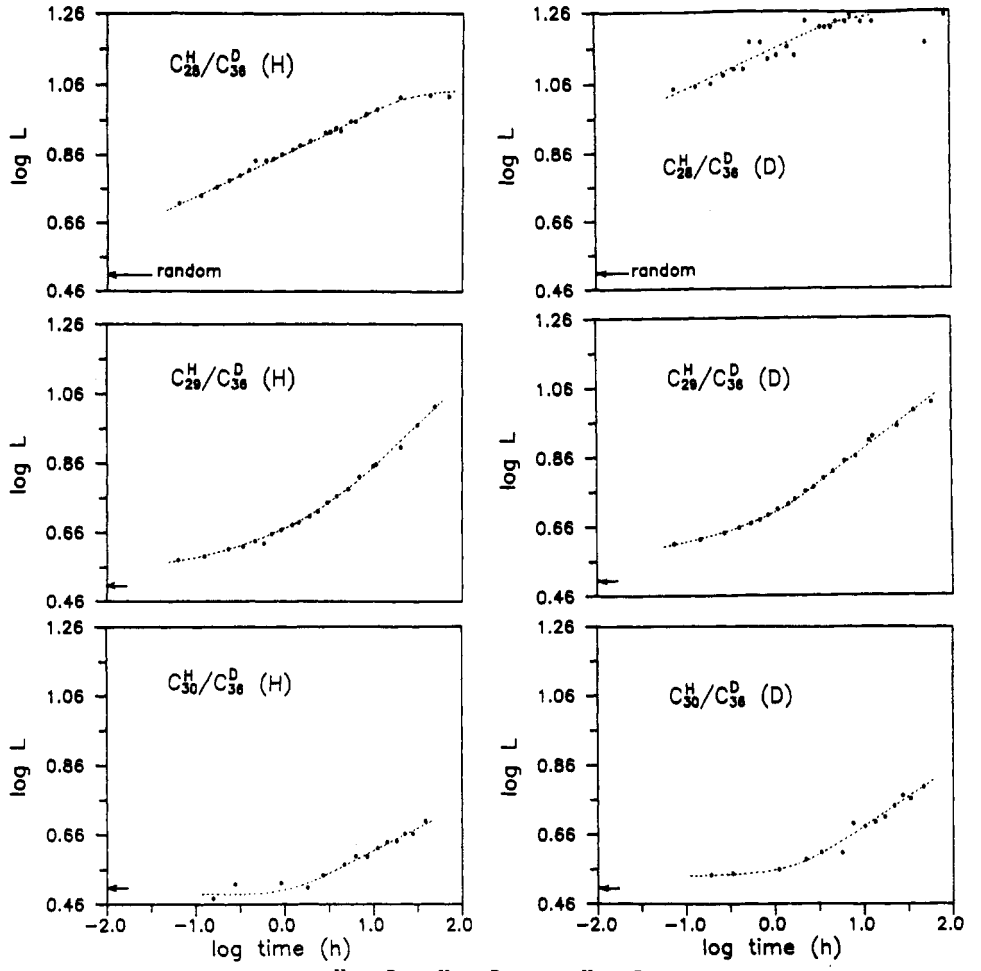

Figure 22. log L plotted against log t for 1:1 mixtures C_{28}^H/C_{36}^D, C_{29}^H/C_{36}^D, and C_{30}^H/C_{36}^D at room temperature. Both components are represented. The estimated value of log L (= 0.51) for random mixing is marked on each plot.

TABLE I: Observed Values of the Slopes of the log L vs log t Curves in the A, B, and C Regions of the C_n^H/C_{36}^D Mixtures

			slopes		
n	concn	component	A	B	C
28	4:1	D		≥0.19	0.02
29		D		0.53	
30		D	0.02	0.37	
28	1:4	H		≥0.34	
28	1:1	H	0.02	0.13	
		D	0.01	0.17	
29		H		0.24	
		D		0.19	
30		H		0.12	
		D		0.11	

as well defined as the π-break. It reflects a tapering-off in the growth rate due to the depletion of small, unstable domains and the beginning of a regime in which large domains grow by the incorporation of smaller ones.[24]

The values of the slopes of the log/log curves are of interest in that they are useful for characterizing the kinetics of the demixing process.[22] Table I lists values in those regions of the log/log plots where measurements seemed meaningful. Measurements in regions A and C were limited to the more or less linear parts of the curve. These gave very small values, less than 0.05. Slopes in region B are most easily measured. For the 4:1 and 1:4 mixtures, the values are in the range 0.30–0.55. Significantly lower values, in the range 0.11–0.24, are found for the 1:1 mixtures.

B. Chain-Length Difference and Concentration Effects. The dependence of the demixing rate on the chain-length difference was estimated for the C_{28}^H/C_{36}^D and C_{29}^H/C_{36}^D mixtures relative to the C_{30}^H/C_{36}^D mixture. The relative rate, as defined earlier, is based on the times that it takes for two mixtures to reach the same state of segregation, as measured by domain size. The rates are found to be enormously dependent on the chain-length difference (Figure 20). For example, the time required for the domains of the minority component in the 4:1 C_{28}^H/C_{36}^D mixture to reach the size, log L = 0.6, is about 1/460 that for the 4:1 C_{30}^H/C_{36}^D mixture; for these same two mixtures but at a concentration ratio 1:4, the contrast is even greater, the rate ratio being 1/1060. For the C_{29}^H/C_{36}^D mixture relative to the C_{30}^H/C_{36}^D mixture, the rate ratio is 1/9.8 for the 4:1 concentration ratio and 1/61.7 for 1:4.

The activation energy difference per methylene group may be estimated from the dependence of the relative rates on the chain length difference. For the 4:1 mixtures near 300 K, this difference is found to be 1.4 kcal/mol on the basis of the rates for the pair of mixtures C_{29}^H/C_{36}^D and C_{30}^H/C_{36}^D; for the pair C_{28}^H/C_{36}^D and C_{30}^H/C_{36}^D, it is 3.7 kcal/mol. For the same mixtures but at a concentration 1:4, the differences are 2.8 and 4.2 kcal/mol, respectively. The average per methylene group is then about 2.0 kcal/mol.

The demixing rates are also dependent on concentration. Over the domain size range 0.55–0.75, a given 1:4 mixture was found to demix faster than the corresponding 4:1 mixture (Figure 21). For example, based on the time needed for domain sizes to reach log L = 0.6, the 1:4 mixture demixes faster than the 4:1 mixture by a factor of about 5 for C_{28}^H/C_{36}^D and about 2 for C_{29}^H/C_{36}^D. For C_{30}^H/C_{36}^D, however, the rates for the 4:1 and 1:4 mixtures are nearly equal.

The generally slower demixing rate for the 4:1 mixture relative to that for the 1:4 mixture is probably a result of the π-break. As noted above, the π-break transition is much more pronounced for the 4:1 mixture, and its effect is to inhibit demixing. However, after the transition, the rate for the 4:1 mixture tends to be greater than for the 1:4 mixture, so that the degree of demixing in the 4:1 advances on that for the 1:4. In the long run, the degree of demixing achieved is comparable for the two mixtures. The

TABLE II: Domain-Size Asymmetry in the 1:1 C_n^H/C_{36}^D Mixtures in Terms of the Normalized Splitting R

n	t, hours	R		$R(C_{36}^D) - R(C_n^H)$
		C_n^H	C_{36}^D	
28	0.3	0.879	0.971	0.092
	4.7	0.930	0.985	0.055
	9.0	0.943	0.985	0.042
29	5.8	0.867	0.900	0.033
	23.0	0.919	0.936	0.017
	35.2	0.939	0.949	0.010
30	3.0	0.705	0.753	0.048
	31.5	0.802	0.856	0.054
	44.0	0.826	0.874	0.048

relative demixing rates displayed in Figure 21 are for the initial stages of the separation, which for the reasons just given favors a faster rate for the 1:4 mixture.

These findings are opposite to expectations that might be inferred from the compositional asymmetry found in phase diagrams for these binary *n*-alkane mixtures at room temperature. These diagrams indicate that at room temperature the mixtures are more stable in the concentration region where the longer chains dominate. The 1:4 mixture is much nearer this region than the 4:1 mixture and therefore might be thought to be the more stable. However, although this asymmetry is clearly apparent in the phase diagram reported for C_{19}/C_{21}[6] and in Mazee's phase diagram for C_{30}/C_{35},[1] it is probably much less significant for the mixtures studied here since the components are less miscible. For our systems at room temperature, the coexistence curve probably is very near the edges of the phase diagram.

C. Domain Sizes and Shapes. Domain sizes converge toward a limiting value as the rates of domain growth level off with time. The convergence is quicker if the mixture is unbalanced in concentration. Thus the time required for the 4:1 and 1:4 mixtures to reach equilibrium is shorter and the limiting domain size smaller than in the case of the 1:1 mixtures.

As noted earlier, a comparison of the average domain sizes for the components making up 1:1 mixtures is interesting because, if the domain shapes are alike for the two components, the average domain sizes must be equal. From the measurement of band splitting, it appears that the average domain sizes of the components are significantly different. However, as we have discussed earlier, band splitting is affected be domain shape. We prefer to account for this discrepancy in these terms.

It appears that the domains of the longer chains are more compact than those of the shorter chains. Table II lists the observed values of the normalized splitting R for the two components as a function of time. The average difference between R for the C_{36}^D domains and that for the C_n^H domains is 0.044 ± 0.022, a reasonable value to be attributed to a difference in domain shapes, since this difference in R is near the value 0.040, which is the change in R that is calculated to occur in going from random-shape domains to square-shape domains, as may be seen from the calibration curve in Figure 4.

A domain-shape asymmetry in which the longer-chain domains are the more compact seems physically plausible. If E_{11} is the pair-interaction energy between extended C_{30}^H chains and E_{22} is that between C_{36}^D chains, then $E_{22} > E_{11}$. With E_{12} designated to be the interaction energy between pairs of unlike chains, we assume $E_{12} \leq E_{11}$; that is, the interaction energy between a short and a long chain is no greater than that between two short chains. Given these conditions, the longer-chain domains will tend to be more compact than those of the shorter chains in order to increase the contribution from E_{22} and decrease that from E_{12}. The shorter chains will then tend to fill in between the more compact longer-chain domains. This picture is consistent with the observation that the difference in domain size is greatest for the C_{28}^H/C_{36}^D mixture, since in that case the inequality between E_{22} and E_{11} is greatest.

D. The Demixing Process. A few comments are in order concerning the nature of the dynamic processes associated with microphase segregation. On the basis of structural similarity alone, it might seem that the demixing mechanism in binary *n*-alkane mixtures would be much more akin to that in polymers than, say, in metals. However, this is not entirely the case. For example, the molecular weights of the *n*-alkanes are sufficiently low that the chain diffusion associated with demixing should be virtually free of the one complication that characterizes polymer diffusion, namely chain entangelment. There are other significant differences that also have their origin in the disparate molecular-weight difference between *n*-alkanes and high polymers. The binary *n*-alkane mixtures, although slightly disordered immediately after the quench, still generally have a high degree of conformational order, are highly crystalline, and have a well defined lamellar structure. Therefore, chain diffusion in *n*-alkane mixtures, in contrast to polymers, takes place in a highly ordered and highly anisotropic environment. In a summary, Table III lists for comparison some of the similarities and differences in the properties and structures of metals, *n*-alkanes, and polymers that may be important in determining the mechanism and kinetics of microphase separation.

TABLE III: Comparison of Property/Structure Factors Associated with the Demixing Process in Binary Mixtures for Metals, *n*-Alkanes, and Polymers

	metals	*n*-alkanes	polymers
constituents	atoms	chains	chains
phase	cryst	cryst	amorph
isotropic	yes	no	yes
conformation	no	yes	yes
entangled	no	no	yes
mechanism	exchange	*a*	reptation

[a] See text.

The vacancy model that has been proposed to account for self diffusion in pure *n*-alkanes[25,26] does not appear to be appropriate for binary mixtures. One serious problem concerns activation energies. The activation energy for self diffusion in pure C_{20} has been determined experimentally and found to be of the order of 80 kcal/mol,[25] a value that has found support in an energy calculation.[26] In contrast, we estimate a much lower value, in the range 10–20 kcal/mol, from measurements on the temperature dependence the demixing rate for the binary mixture C_{30}^H/C_{36}^D.[19]

One possible diffusion model that does seem appropriate for unstable binary *n*-alkane mixtures is one intermediate between the vacancy and reptation models. It seems likely that chain transport in the binary mixture is primarily in the longitudinal direction, in view of the considerable evidence indicating this is the case in the high-temperature crystalline phases of the *n*-alkanes[6] and in polymer crystals as well.[15] (In contrast to the situation in lipid bilayers, for example, where lateral movement dominates[27].) Large-scale longitudinal excursions of the chains in a binary mixture would be made possible by the presence of the partial vacancies that must exist in the interlayer regions. These partial vacancies, which must migrate about, would provide transient paths for chain migration via reptation. As the demixing progressed and the domains became larger and the crystals more ordered, the concentration of partial vacancies would decrease. This may be an additional factor that causes the demixing process to slow down with time.

Acknowledgment. This research was supported by the National Institutes of Health (GM 27690). We would like to thank Dr. Yesook Kim for help in measuring the infrared spectra and Dr. Douglas Cates for technical assistance.

References and Notes

(1) Mazee, W. M. *Prepr.—Am. Chem. Soc. Div. Pet. Chem.* **1958**, *3* (4), 35.
(2) Dorset, D. L. *Macromolecules* **1986**, *19*, 2965.
(3) Dorset, D. L. *Macromolecules* **1990**, *23*, 623.
(4) Snyder, R. G.; Kim, Yesook; Strauss, H. L.; Goh, M. C. *Prepr.—Am. Chem. Soc. Div. Polym. Chem.* **1989**, *30*, 295.
(5) White, J. W.; Dorset, D. L.; Epperson, J. E.; Snyder, R. G. *Chem. Phys. Lett.* **1990**, *166*, 560.
(6) Maroncelli, M.; Strauss, H. L.; Snyder, R. G. *J. Phys. Chem.* **1985**, *89*, 5260.

(7) Kim, Yesook; Strauss, H. L.; Snyder, R. G. *J. Phys. Chem.* **1989**, *93*, 485.
(8) Hiebert, G. L.; Hornig, D. F. *J. Chem. Phys.* **1952**, *20*, 918.
(9) Tasumi, M.; Krimm, S. *J. Polym. Sci. Part A2* **1968**, *6*, 995. Spells, S. J.; Sadler, D. M.; Keller, A. *Polymer* **1980**, *21*, 1121.
(10) Snyder, R. G. *J. Mol. Spectrosc.* **1961**, *7*, 116. Tasumi, M.; Shimanouchi, T. *J. Chem. Phys.* **1965**, *43*, 1245.
(11) Smith, A. E. *J. Chem. Phys.* **1953**, *21*, 2229.
(12) Buckingham, A. D.; Hentschel, H. G. E. *J. Polym. Sci. Phys. Ed.* **1980**, *18*, 853.
(13) Spells, S. J.; Sadler, D. M. *Polymer* **1984**, *25*, 739. English, A. D.; Smith, P.; Axelson, D. E. *Polymer* **1985**, *26*, 1523.
(14) Hornig, D. F.; Hiebert, G. L. *J. Chem. Phys.* **1957**, *27*, 752.
(15) Guillaume, F.; Doucet, J.; Sourisseau, C.; Dianoux, A. J. *J. Chem. Phys.* **1989**, *91*, 2555; Piesczek, W.; Strobl, G. R.; Malzahn, K. *Acta Cryst. Part B* **1974**, *30*, 1278; Strobl, G.; Ewen, B.; Fischer, E. W.; Piesczek, W. *J. Chem. Phys.* **1974**, *61*, 5257.
(16) Dorset, D. L. *Macromolecules* **1987**, *20*, 2782.
(17) Snyder, R. G.; Maroncelli, M.; Qi, S. P.; Strauss, H. L. *Science* **1981**, *214*, 188.
(18) Matheson, R. R.; Smith, P. *Polymer* **1985**, *26*, 289.
(19) Snyder, R. G. Unpublished results.
(20) Gunton, J. D.; San Miguel, M.; Sahni, P. S. In *Phase Transitions and Critical Phenomenon*; Domb, C., Lebow, J. L., Eds.; Academic Press: New York, 1983; Vol. 8. Binder, K.; Kalos, M. H. In *Monte Carlo Methods in Statistical Physics*; Binder, K., Ed.; Springer-Verlag: New York, 1986; Chapter 6.
(21) Butler, E. P.; Thomas, G. *Acta Met.* **1970**, *18*, 947. Bouchard, M.; Thomas, G. *Acta Met.* **1975**, *23*, 1485.
(22) Snyder, H. L.; Meakin, P. *J. Chem. Phys.* **1983**, *79*, 5588.
(23) Snyder, R. G.; Conti, G.; Strauss, H. L. To be published.
(24) Lifshitz, I. M.; Slyozov, V. V. *J. Phys. Chem. Solids* **1961**, *19*, 35.
(25) Narang, R. S.; Sherwood, J. N. *Mol. Cryst. Liq. Cryst.* **1980**, *59*, 167.
(26) Farmer, B. L.; Eby, R. K. *Polymer* **1987**, *28*, 86.
(27) Lange, Y. In *The Physical Chemistry of Lipids*; Small, D. M., Ed.; Plenum Press: New York, 1986; Chapter 13.

Ion-Selective Properties of a Small Ionophore in Methanol Studied by Free Energy Perturbation Simulations

Johan Åqvist,*

Department of Molecular Biology, Uppsala Biomedical Centre, Box 590, Uppsala University, S-75124 Uppsala, Sweden

Osvaldo Alvarez,

Department of Biology, Faculty of Sciences, University of Chile, Santiago, Chile

and George Eisenman

Department of Physiology, UCLA Medical School, Los Angeles, California 90024-1751
(Received: May 18, 1992)

The ion-selective properties of the cyclic depsipeptide molecule *valinomycin* in methanol are studied by free energy perturbation molecular dynamics simulations. The dependence of the alkali cation selectivity on the dipole moment of the backbone carbonyl groups that ligate the ion is examined and found to behave in a systematic way. Since available force fields have not been parametrized for this type of ion–carbonyl interaction, the results are used to determine carbonyl partial charges that reproduce the observed selectivity quantitatively. The optimal dipole moment is somewhat higher than that normally used in molecular mechanics force fields and indicates that there is a significant polarization of the carbonyl groups by the field from the ion. The simulations also suggest that the unloading of ions mainly would occur through the lactic acid face of the molecule since it does not provide as effective a shield against attack from the solvent as the more hydrophobic isohydroxyvaleric acid face.

Introduction

The principles underlying molecular recognition in membrane channels and ion carriers constitute an issue of fundamental interest in molecular biophysics. During the past years considerable progress has been made in advancing our understanding of recognition and selectivity phenomena both in biomolecular and synthetic organic systems.[1] With modern computational techniques it has also become possible to study these phenomena on a detailed microscopic level of description.[2] Unfortunately, we are still lacking accurate structural information for many of the biologically most interesting systems and in particular for transmembrane ion channels. However, there are several simpler systems which display nontrivial selectivity properties of essentially the same type as observed in biological channels and, from the viewpoint of theoretical chemistry, they can serve as useful test cases that allow us to judge the reliability of computational models and procedures. Needless to say, it is of great importance to be able to really gauge the accuracy of molecular mechanics force fields in cases where extensive experimental data is available. It is also necessary to consider both structure and energetics (and for some purposes also dynamics) when assessing the reliability of a given force field. Structural analysis based on molecular dynamics (MD) or Monte Carlo (MC) simulations provides a more stringent test than "static" energy minimization methods, since the former correspond to a more realistic situation in which the system has a certain (nonzero) thermal energy. This allows for a sampling of the available conformational space and the calculation of time- or ensemble-averaged structures. By employing free energy perturbation (FEP) simulations, it is also possible to make direct comparisons of energetics to experiments in solution.

In this paper we address the problem of ion binding and selectivity for the small ion carrier valinomycin. This molecule has the ability to bind small monovalent cations rather tightly in various solvents. For the alkali cation series it has the selectivity sequence Rb > K > Cs > Na > Li, which is nontrivial in the sense that an ion in the middle of the series is selected. We report FEP/MD simulations of the complexation of alkali ions with valinomycin in methanol, for which the most extensive set of experimental data is available. By varying key parameters of the force field we show that it is possible to identify the factors that give rise to particular selectivity patterns. The ion-selective properties of valinomycin are found to behave in a systematic way as a function of the ligand field strength (or dipole moment), as has been predicted earlier.[3]

Structure and Energetics of Valinomycin Complexes

The primary structure of valinomycin is cyclo-(-D-Hyl-D-Val-L-Lac-L-Val-)$_3$, where D-Hyl is D-hydroxyisovaleric acid, L-Lac is L-lactic acid, and Val denotes valine. In solvents of low dielectric

0022-3654/92/2096-10019$03.00/0